Mesoscale description of an asymmetric lamellar phase

V. Kumaran[a)]
Department of Chemical Engineering, Indian Institute of Science, Bangalore 560 012, India

(Received 12 March 2009; accepted 1 May 2009; published online 10 June 2009)

The relationship between the parameters in a description based on a mesoscale free energy functional for the concentration field and the macroscopic properties, such as the bending and compression moduli and the permeation constant, are examined for an asymmetric lamellar phase where the mass fractions of the hydrophobic and hydrophilic parts are not equal. The difference in the mass fractions is incorporated using a cubic term in the free energy functional, in addition to the usual quadratic and quartic terms in the Landau–Ginsburg formulation. The relationship between the coefficient of the cubic term and the difference in the mass fractions of the hydrophilic and hydrophobic parts is obtained. For a lamellar phase, it is important to ensure that the surface tension is zero due to symmetry considerations. The relationship between the parameters in the free energy functional for zero surface tension is derived. When the interface between the hydrophilic and hydrophobic parts is diffuse, it is found that the bending and compression moduli, scaled by the parameters in the free energy functional, do increase as the asymmetry in the bilayer increases. When the interface between the hydrophilic and hydrophobic parts is sharp, the scaled bending and compression moduli show no dependence on the asymmetry in the bilayer. The ratio of the permeation constant in between the water and bilayer in a molecular description and the Onsager coefficient in the mesoscale description is $O(1)$ for both sharp and diffuse interfaces and it increases as the difference in the mass fractions is increased. © *2009 American Institute of Physics*.
[DOI: 10.1063/1.3143183]

I. INTRODUCTION

Surfactant solutions are often encountered in industrial applications. Depending on the relative concentrations of water and surfactant, these self-assemble into micelles, lamellar or hexagonal phases. These surfactants mesophases are anisotropic materials, which have fluidlike disorder in some directions and solidlike ordering in other directions.[1] In order to be able to accurately model these systems, it is necessary to have a good understanding of the relationship between the rheology and the structure of the fluid. The evolution of these systems to an equilibrium state is kinetically constrained, because the energy required for rearrangements is much larger than the thermal energy. Even though a perfect defect free stack of layers is the final equilibrium state, real samples are rarely defect free due to kinetic constraints. These fluids could be ordered by the application of shear. However, the viscosity (and shear moduli) depends on the structure and state of ordering in the system, and the state of ordering depends on the shear history. For this reason, isotropic non-Newtonian constitutive equations[2] are not sufficient for these systems and it is necessary to include additional fields (such as the unit normal to the layers) to accurately describe their rheology. It is unrealistic to attempt a microscopic simulation for these fluids, because the lamellar spacing is typically small compared to macroscopic scales (the distance between layers in lyotropic liquid crystalline phases is usually a few hundred angstroms). Since the rheology of the liquid depends on the structure, it is difficult to obtain closed form equations for the density and momentum fields alone in these systems.

It is computationally infeasible to simulate more than a single bilayer using these molecular dynamics simulations and so a mesoscale simulation technique is required to bridge the gap between the molecular simulations and the macroscopic applications. For a mesoscale simulation, which resolves a few lamellae,[3–9] the fundamental dynamical quantity is the concentration (order-parameter) field, which is the difference in the concentrations between the hydrophilic and hydrophobic parts (the sum of the concentrations is a constant if the fluid is incompressible). However, a mesoscale simulation procedure is not useful for making quantitative predictions unless a connection can be made between properties, which can be measured in molecular simulations, such as the layer bending modulus and the permeation constant, and the parameters in the free energy functional. This connection was established for a symmetric lamellar phase (equal mass fractions of hydrophilic and hydrophobic parts) recently.[9] In the present study, we analyze the same for an asymmetric bilayer, in which the mass fractions of the hydrophilic and hydrophobic parts are not equal.[10–14]

The order parameter in a mesoscale description is the concentration field ψ, which is defined as $\psi=(c_w-c_o)/(c_w+c_o)$, where c_w and c_o are the concentrations of the hydrophilic and hydrophobic components (the total concentration c_w+c_o is a constant for an incompressible system). The free energy functional for the order parameter is chosen so that a periodic modulation in ψ of wavelength equal to the

[a)]Electronic mail: kumaran@chemeng.iisc.ernet.in.

layer spacing is obtained at equilibrium. Most earlier studies[4–6,8,9] focused on a "symmetric" free energy functional, for which the mass fractions of the hydrophilic and hydrophobic parts are equal. This is due because a symmetric lamellar phase is an equilibrium solution for a Landau–Ginzburg type free energy functional, which contains terms proportional to the second and fourth powers of the concentration, in addition to a term that promotes periodic modulation of the concentration field. The relation between the molecular and mesoscale parameters for a symmetric lamellar phase has been formulated.[9] However, most surfactant lamellar phases are not symmetric and the difference in the mass fractions of the hydrophilic and hydrophobic parts could be significant. Surfactant lamellar phases often swell when the water content is increased and the ratio of the mass fractions of surfactant and water decreases. Multiscale modeling of lamellar mesophases will be successful only if this asymmetry can be incorporated into a mesoscale description. Here, we examine the formulation of the mesoscale description, which incorporates the difference in the mass fractions of the hydrophilic and hydrophobic parts, and examine how this asymmetry affects the thermodynamic and dynamical properties of the lamellar phase.

In order to model an asymmetric lamellar phase, a term proportional to the third power of the concentration is incorporated into the free energy functional. The other parameters in the free energy functional[9] are an energy scale (the concentration field is defined to be dimensionless as above) and a parameter r, which determines the sharpness of the interface between the hydrophilic and hydrophobic parts. The concentration profile is close to a sine wave for $r \gg 1$, while it approaches a step function for $r \ll 1$. The parameter r in the mesoscale description can be directly obtained from the concentration profile of the hydrophilic and hydrophobic parts in molecular simulations.[9] The energy scale in the free energy functional is related to the molecular simulation using the fluctuation response of the bilayers. Fluctuations in an ordered lamellar phase can be of two types: Layer compression in the direction perpendicular to the plane of the layers and layer bending along the plane of the layers. The stress due to the layer compression is proportional to the product of the "compression modulus" and the second spatial derivative of the layer displacement field along the layer normal direction. For a tensionless membrane, the stress due to bending is proportional to the "bending modulus" and the fourth spatial derivative of the layer displacement field. The bending modulus can be obtained in molecular simulations from the structure factor for the height-height correlations. Using a relation between the energy scale in the free energy functional and the bending modulus, the energy scale in the free energy functional can be extracted from a molecular simulation.[9] Here, we also show how the coefficient of the cubic term in the free energy functional can be related to the difference in the mass fractions of the hydrophilic and hydrophobic parts.

The dynamics of the system is governed by dynamical equations for the concentration and velocity fields. The parameters determining the dynamical response are the Onsager coefficient for the concentration field and the viscosity in the fluid momentum equation. In the mesoscale description, there are two dynamical parameters, the Onsager coefficient for the concentration field and the kinematic viscosity in the fluid momentum equation. The Onsager coefficient is related to the relative motion of the hydrophilic and hydrophobic parts; the equivalent phenomenon at the molecular scale is the permeation of the water through the hydrophobic bilayer. The relationship between the Onsager coefficient and the permeation constant was obtained for a symmetric bilayer earlier;[9] here we carry out the same calculation for an asymmetric bilayer and examine the dependence of the ratio of the permeation constant and Onsager coefficient on the difference in the mass fractions of the hydrophilic and hydrophobic parts.

An important concern in the mesoscale description of lamellar phases is that the model should predict a zero surface tension, since a lamellar phase has no surface tension. The free energy functional[6,8] for a symmetric bilayer will have zero surface tension only when the interfacial profile is sinusoidal. As the interface sharpness increases, it is necessary to add a surface tension term to the free energy functional in order to obtain zero surface tension. The coefficient of the surface tension term required for zero surface tension for a symmetric bilayer was calculated earlier.[9] Here, we calculate the coefficient for an asymmetric bilayer.

In Sec. II, the relationship between the parameters in the free energy functional and the shape of the concentration profile is first examined. The coefficient of the cubic term in the free energy functional is related to the asymmetry in the concentration profile both in the limits of very sharp interfaces and very diffuse interfaces.

II. ANALYSIS

The free energy functional for the concentration field in the mesoscale description, required to produce a lamellar phase as the equilibrium solution, is

$$F[\psi] = A\int dV\left(-\frac{\psi^2}{2}+\frac{c\psi^3}{3}+\frac{\psi^4}{4}+\frac{g}{2k^2}(\nabla\psi)^2 + \frac{r}{2k^4}((\nabla^2+k^2)\psi)^2\right). \quad (1)$$

Here, we defined the concentration field ψ and the parameters g and r to be dimensionless, while k has dimensions of the inverse of length. Parameter A represents an energy density (energy per unit volume) and sets the energy scale in the system. The first and third terms on the right side of the above equation are the usual quadratic and quartic terms in a Landau–Ginzburg free energy, which results in segregation in a binary fluid due to the negative sign in the first term, while the second term is a cubic contribution to the free energy functional, which accounts for the asymmetry in the concentration profile. The fourth term on the right side is the surface tension terms, while the last term promotes the formation of interfaces with wavelength $(2\pi/k)$.

The macroscopic dynamics of the lamellar phase is described by the local direction of the unit normal to the layers **n**, which is perpendicular to the plane of the layers, and the

local displacement field u, which provides the local displacement of layers from their equilibrium positions. The free energy changes and the stresses generated depend only on the variation in u in the directions tangential and normal to the layers, since the system is at equilibrium when u is zero. In order to write down the free energy for small displacements, we choose a coordinate system in which the coordinates x and y are locally tangential to the layers and z is perpendicular to the plane or the layers. The partial derivatives are defined as $u_x=(\partial u/\partial x)$, $u_y=(\partial u/\partial y)$, and $u_z=(\partial u/\partial z)$; a larger number of subscripts represents repeated derivatives with respect to the position variables. The free energy functional for this correct to second order in u can be written, using symmetry arguments, as

$$F[u] = F_0 + \int dV \left(\frac{Bu_z^2}{2} + \frac{G(u_x^2 + u_y^2)}{2} + \frac{K(u_{xx} + u_{yy} + u_{zz})^2}{2} \right). \tag{2}$$

Here, the first term in the integral on the right side of Eq. (2) imposes a penalty for displacements normal to the layers, which tend to compress or expand the layers, and B is the layer compression modulus. The second term in the integral on the right side of Eq. (2) represents the free energy change due to a change in area along the layers and G is the surface tension. The third term in the integral on the right is the change in energy due to bending of the interface and K is the curvature modulus.

In a real lyotropic liquid crystalline fluid, the surface tension is zero. Our analysis[9] shows that when we do coarse graining of a free energy functional of the type Eq. (2), with $g=0$, we obtain a nonzero value of G in Eq. (2) in the most general case. In the analysis, we determine the value of $g=g_0$, where g_0 is a negative real number, to be used in the simulations so that the macroscopic surface tension is zero. This is discussed a little later.

A. Concentration profiles

The concentration profile for the equilibrium state is obtained by minimizing $F[\psi]$ with respect to variations in ψ,

$$\frac{\delta F}{\delta \psi} = 0. \tag{3}$$

Using the Euler–Lagrange equations, we obtain the following cubic form for the concentration field ψ:

$$-\psi + c\psi^2 + \psi^3 - g\nabla^2\psi + r(\nabla^4 + 2k^2\nabla^2 + k^4)\psi = 0. \tag{4}$$

First, we note that the last term on the left side of Eq. (4) is zero for a sinusoidal variation with wave number k, therefore if r is large; we would expect the equilibrium profile to be a sinusoidal modulation with wave number k. However, there will be a generation of higher harmonics due to the first two terms on the left side of Eq. (4) and the most general concentration profile will be of the form,

$$\psi = \sum_{n=-\infty}^{\infty} \psi_n \exp(\imath nkz), \tag{5}$$

where n is an integer. This is inserted into Eq. (4) and the coefficients of the terms with equal powers of $\exp(\imath nkz)$ are set equal to zero in order to obtain solutions for ψ_n, which are a function of r. Since the concentration field is real, $\psi_{-n}=\psi_n$. Also, the coefficient ψ_0 is not zero, in general, because the concentration profile is asymmetric. The value of the coefficient ψ_0 is evaluated from the total mass condition,

$$\frac{1}{\lambda}\int_0^{\lambda} dz\psi(z) = \psi_0, \tag{6}$$

where $\lambda=(2\pi/k)$ is the wavelength of the concentration modulation, or the layer spacing. Thus, the first coefficient ψ_0 is fixed from knowledge of the total concentration. The determination of the higher coefficients is discussed next.

In the limit $r \gg 1$, the fifth term on the left side of Eq. (4) is large compared to the other terms and so we would expect the solution to be close to a sine wave. However, due to the condition on the total concentration, a symmetric sine wave is not a solution of Eq. (4). We can use an asymptotic expansion in the parameter r^{-1} as follows. In this expansion, it is clear that ψ_1 has to be $O(1)$ in order to generate a wave. The magnitude of the higher terms for $n>1$ can be obtained by inserting Eq. (5) into Eq. (4) and examining coefficients of $\exp(\imath nkz)$ in the resulting equation. Consider the equations for ψ_0, ψ_1, and ψ_2, that is, the expansion (4) for $n=0$, $n=1$, and $n=2$. If we retain only the leading order terms in r and c and assume $\psi_2 \ll \psi_1$ and $\psi_0 \ll \psi_1$, then we obtain

$$r\psi_0 + 2c\psi_1^2 = 0, \tag{7}$$

$$(-1 - g + 2(\psi_0 + \psi_2)c + 3\psi_1^2) = 0, \tag{8}$$

$$9r\psi_2 + c\psi_1^2 = 0. \tag{9}$$

The equations are self-consistent only if $\psi_0 \sim \psi_2 \sim r^{-1/2}$ and $c \sim r^{1/2}$. A more detailed examination of the hierarchy of equations reveals that all higher order coefficients, ψ_n for $n \geq 3$, are $O(r^{-1})$ or smaller. The above Eqs. (7)–(9) can be solved simultaneously to obtain ψ_1 and the coefficient c in the free energy functional 1. Note that the coefficient ψ_0 has already been determined from the total mass condition (6). Solving Eqs. (7) and (8) simultaneously, we obtain a quartic equation for ψ_1 as

$$54\psi_1^4 - 18\psi_1^2(1+g) - 19(\psi_0^2/r) = 0. \tag{10}$$

This equation can be solved to obtain the solution for ψ_1,

$$\psi_1^2 = \frac{1+g}{6} + \frac{\sqrt{9(1+g)^2 + 114(\psi_0^2/r)}}{18}. \tag{11}$$

Using solution (11), we can obtain c as a function of ψ_0 from Eq. (7),

$$c = -\frac{r\psi_0}{2\psi_1^2}, \tag{12}$$

and ψ_2 from Eq. (9),

$$\psi_2 = \frac{\psi_0}{18}. \tag{13}$$

Note that $c \sim r^{1/2}$ and $\psi_2 \sim r^{-1/2}$, as anticipated earlier. The higher coefficients in the expansion can be systematically determined. In particular, we find that

$$\psi_3 = -\frac{c\psi_2\psi_1}{32r} - \frac{\psi_1^3}{64r}, \tag{14}$$

$$\psi_4 = -\frac{c\psi_2^2 - 2c\psi_1\psi_3 - 3\psi_1^2\psi_2}{225r}. \tag{15}$$

Note that $\psi_3 \sim r^{-1}$ and $\psi_4 \sim r^{-3/2}$. In fact, we can show that $\psi_n \sim r^{(n-1)/2}$ in the asymptotic expansion.

In the limit $r \ll 1$, we expect a sharp interface between the hydrophilic and hydrophobic regions. The limiting profile in this limit would be expected to be of the form,

$$\psi = 1 \quad \text{for} \quad 0 < (z/\lambda) < (a/2) = -1 \quad \text{for} \quad (a/2) < (z/\lambda) < (1-a/2) = 1 \quad \text{for} \quad (1-a/2) < (z/\lambda) < 1, \tag{16}$$

where λ is the wavelength of the perturbations. Here, the bilayer is symmetric for $a=0.5$ and is asymmetric for $a \neq 0.5$. We consider that $a > 0.5$ without loss of generality. The coefficients ψ_n in Eq. (5) are easily evaluated using the orthogonality conditions for the cosine functions,

$$\psi_0 = 2a - 1, \tag{17}$$

and

$$\psi_n = \frac{2\sin(an\pi)}{\pi n}, \tag{18}$$

for $n \geq 1$. The coefficient c in the free energy functional is evaluated from the z-independent component of Eq. (4),

$$c = \frac{-\psi_0 + \psi_0^3 + 6\psi_0\Sigma_{n=1}^{\infty}\psi_n^2 + 2\Sigma_{n=1}^{\infty}\Sigma_{m=1}^{\infty}(\psi_n\psi_m\psi_{-n-m} + \psi_{-n}\psi_{-m}\psi_{n+m})}{\psi_0^2 + 2\Sigma_{n=1}^{\infty}\psi_n^2}. \tag{19}$$

The limiting value of c for $r \gg 1$ is given by Eq. (12). The limiting value of c for $r \ll 1$ can be obtained using the asymptotic expressions for the coefficients ψ_n in Eq. (18). Since the sums are convergent for $n \to \infty$, the numerical approximation was obtained using 200 terms in the series for the sums $\Sigma_{n=1}^{\infty}\psi_n^2$ and $\Sigma_{n=1}^{\infty}\Sigma_{m=1}^{\infty}\psi_n\psi_m\psi_{-n-m}$. These are shown as a function of ψ_0, along with the coefficient c determined from Eq. 19 in Fig. 1.

The coefficients ψ_n and the concentration profiles were evaluated numerically for "zero surface tension" case for which g and r are related as shown in Eq. (4) a little later.

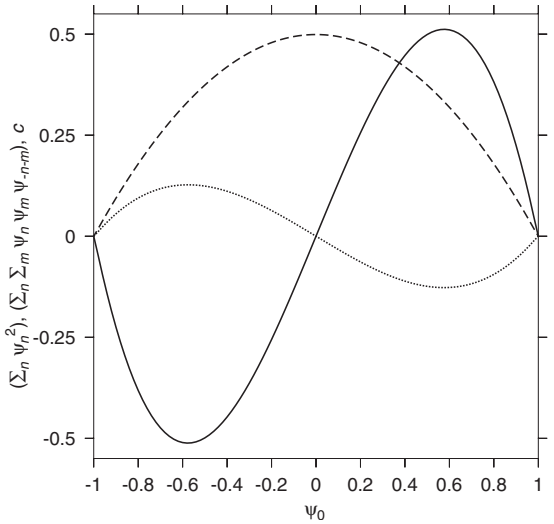

FIG. 1. The summations $\Sigma_{n=1}^{200}\psi_n^2$ (dashed line) and $\Sigma_{n=1}^{200}\Sigma_{m=1}^{200}\psi_n\psi_m\psi_{-n-m}$ (dotted line) using the coefficients ψ_n in Eq. (18), along with the coefficient c (solid line) determined from Eq. (19), as a function of ψ_0.

The coefficients are different for the zero surface tension case because the bilayers described by the free energy functional 1 has a positive surface tension for $g=0$ and it is necessary to set g equal to a negative value for the zero tension state. The coefficients ψ_n were numerically evaluated as follows. The series in Eq. (4) was truncated at $n=8$ and eight simultaneous nonlinear equations were obtained. These were solved iteratively using the Newton–Raphson procedure in order to obtain the coefficients ψ_n from $n=1$ to $n=8$. In the iterative procedure, the initial guesses for the coefficients were chosen as follows. In the limit $r \gg 1$, the first, second, and third terms on the left of Eq. (4) can be neglected in comparison to the last term and the solution for the concentration field is a cosine wave with wave number k. The coefficient ψ_0 is determined by the asymmetry in the bilayer from Eq. (6), while the initial guesses for coefficients ψ_1, ψ_2, and the coefficient c in the free energy functional (1) are obtained by solving Eqs. (7)–(9), while the initial guesses for all other coefficients are set equal to zero. Using these initial guesses, the equations obtained by inserting Eq. (5) in Eq. (4) are solved simultaneously using the Newton–Raphson procedure to determine the coefficients ψ_n. Once the coefficients for a large value of $r=10$ are determined, the parameter r was progressively reduced by factors of 2 using the solution for a given value of r as the starting guess for $(r/2)$, in order to obtain the coefficients ψ_n. These coefficients are shown as a function of r in Fig. 2. The solutions in the limit $r \gg 1$, 11, and 13 require that $\psi_0 \sim r^{-1/2}$. Therefore, in Fig. 2, we set $\psi_0 = (0.25/r^{1/2})$ and $(0.5/r^{1/2})$ for $r \geq 1$, and $\psi_0 = 0.25$ and 0.5 for $r \leq 1$. The concentration profiles obtained for different values of r are shown in Fig. 3. As an-

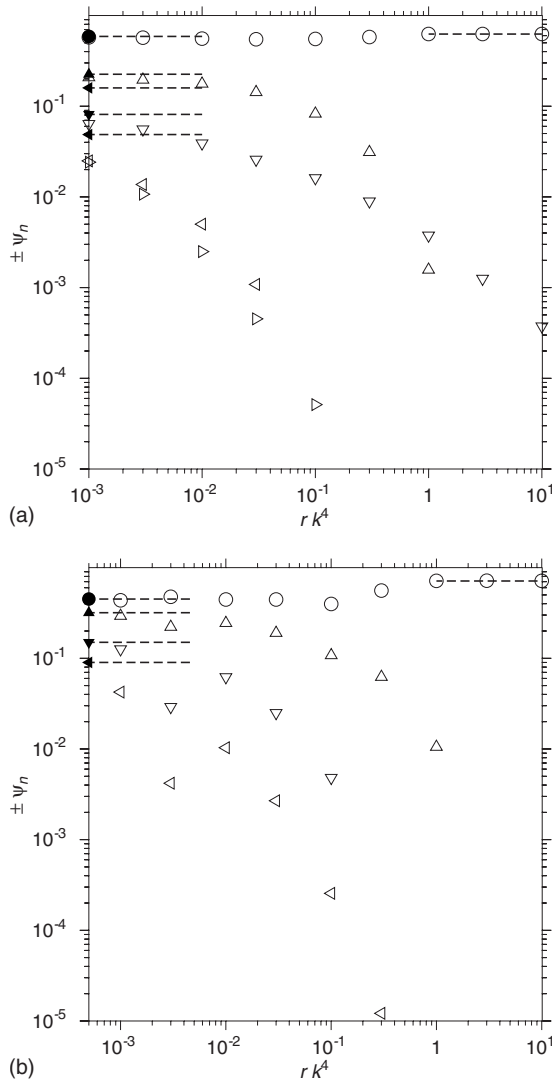

FIG. 2. The coefficients $\pm\psi_n$ as a function of the parameter r. ○ denotes ψ_1, △ denotes ψ_2, ▽ denotes ψ_3, ▷ denotes ψ_4, and ◁ denotes ψ_5 for an asymmetric bilayer with zero surface tension with $\psi_0=(0.25/r^{1/2})$ for $r\geq 1$ and $\psi_0=0.25$ for $r\leq 1$ (a), and $\psi_0=(0.5/r^{1/2})$ for $r\geq 1$ and 0.5 for $r\leq 1$ (b). The bold symbols and dashed lines on the left show the asymptotic values for $r\ll 1$ form Eq. (18). The line on the right shows the asymptotic value for ψ_1, for $r\gg 1$.

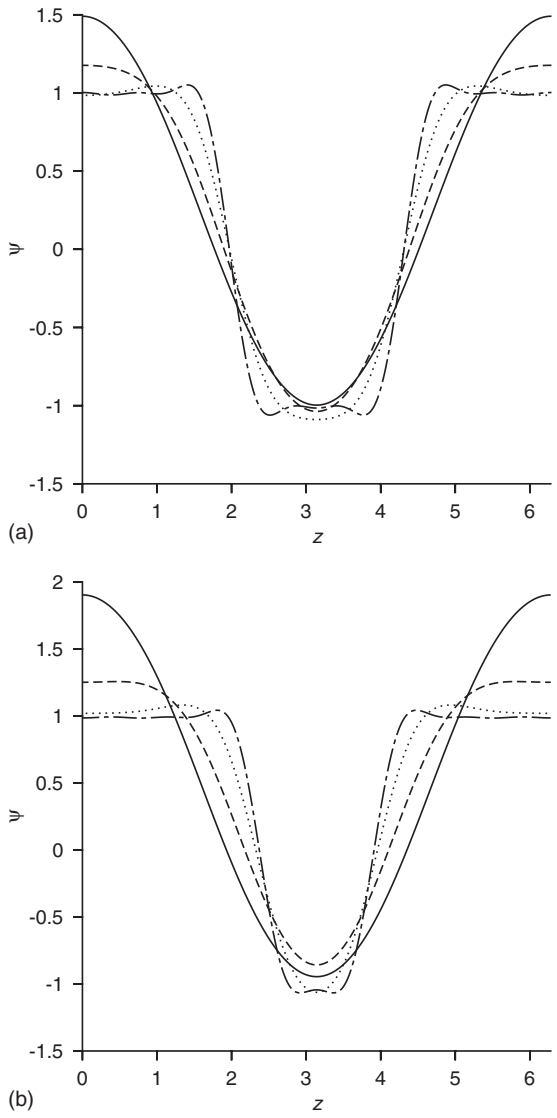

FIG. 3. The concentration ψ as a function of distance z for different values of the parameter r for an asymmetric bilayer with (a) $\psi_0=0.25$ and (b) $\psi_0=0.5$. Solid line denotes $r=1$, dashed line denotes $r=10^{-1}$, dotted line denotes $r=10^{-2}$, and dot-dash line denotes $r=10^{-3}$.

ticipated, the concentration profile is close to a sinusoidal profile for $r\geq 1$, but becomes close to a step profile as r decreases.

B. Bending and compression moduli

The layer compression and bending moduli are extracted from the free energy functional, Eq. (1), using a small perturbation about the equilibrium solution of the form

$$\psi=\sum_{n=-\infty}^{\infty}\psi_n\exp(\imath nk(z-u(x,y,z,t))), \tag{20}$$

where u is the layer displacement field in the z direction. The above expansions are inserted into the free energy functional (1), expand in a series in small u, and include terms that are quadratic in u and its derivatives. Further, we assume that the length scale for the variation in the u field is large compared to the layer spacing $\lambda=(2\pi/k)$. If we integrate over lengths comparable to the λ to obtain a coarse-grained free energy functional, all terms in the free energy functional proportional to $\exp(\imath mkz)$ for $m\neq 0$ will average to zero. Then, we will be left only with terms which do not have any modulation over distances comparable to λ; we recover a free energy functional of the form (2). The details of the calculation are given in an earlier publication[9] and the final results for the constants B, K, and G are

$$B=A\sum_{n=-\infty}^{\infty}(2rn^2(3n^2-1)+gn^2)\psi_n^2,$$

$$K=A\sum_{n=-\infty}^{\infty}(rn^2/k^2)\psi_n^2, \tag{21}$$

$$G=A\sum_{n=-\infty}^{\infty}(2rn^2(n^2-1)+gn^2)\psi_n^2.$$

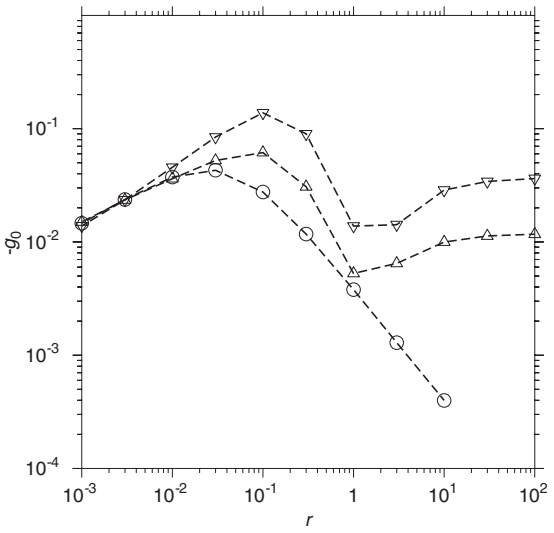

FIG. 4. The variation in $-g_0$ with r, where g_0 is the value of g in the free energy functional (1), which corresponds to a zero tension state for a symmetric bilayer (○) $\psi_0=(0.25/r^{1/2})$ for $r\geq 1$, $\psi_0=0.25$ for $r\leq 1$ (△), and $\psi_0=(0.5/r^{1/2})$ for $r\geq 1$ and 0.5 for $r\leq 1$ (▽).

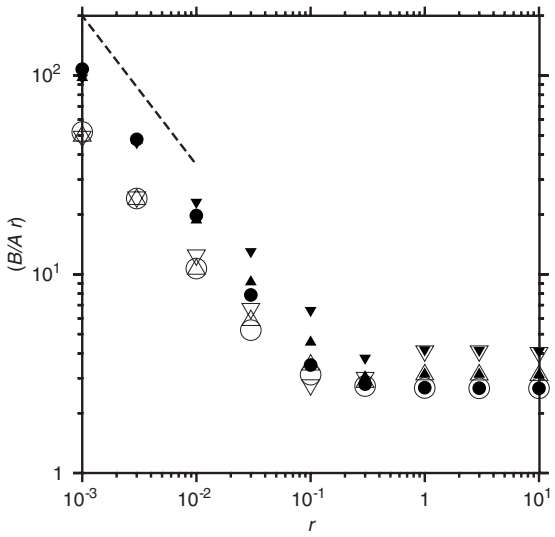

FIG. 5. The scaled compression modulus $(B/(Ar))$ for a symmetric bilayer (○), for an asymmetric bilayer with $\psi_0=(0.25/r^{1/2})$ for $r\geq 1$, and $\psi_0=0.25$ for $r\leq 1$ (△), and an asymmetric bilayer with $\psi_0=(0.5/r^{1/2})$ for $r\geq 1$ and 0.5 for $r\leq 1$ (▽). The filled symbols show the results for zero surface tension, and the filled symbols show the results for $g=0$. The dashed line on the left shows a slopes of -0.75.

The surface tension in the macroscopic description has contributions from both the term proportional to r and the term proportional to g in the free energy functional (1), whereas the bending modulus depends only on r. In order to achieve a tensionless state, it is necessary to construct the free energy functional with the parameter g chosen, so that

$$g = g_0 = -\frac{\Sigma_{n=-\infty}^{\infty} 2rn^2(n^2-1)\psi_n^2}{\Sigma_{n=-\infty}^{\infty} n^2\psi_n^2}. \tag{22}$$

For this choice of parameters, the bending modulus would be

$$B = A\sum_{n=-\infty}^{\infty} 4rn^4\psi_n^2. \tag{23}$$

Figure 4 shows $-g_0$ as a function of r for both the symmetric and asymmetric bilayers. In the limit $r\ll 1$, we found that $g_0\propto r^{1/2}$ for both symmetric and asymmetric bilayers. The physical reasons for the scaling behavior of g_0 in the limits $r\gg 1$ and $r\ll 1$ is as follows:

(1) For a perfect step function $(r=0)$, the coefficients ψ_n decrease proportional to $(1/n)$. However, when r is small but nonzero, Eq. (18) is valid only for $n\ll r^{-1/4}$. This is because Eq. (18) was obtained assuming that the term proportional to r in Eq. (4) can be neglected. For a small but nonzero value of r, the term proportional to r on the left side of Eq. (4) becomes comparable to the other terms for $n\sim r^{-1/4}$. This can be adequately represented by a cutoff at $n\sim r^{-1/4}$ of the series expansion (22), when ψ_n is given by Eq. (18). When this upper limit for n is inserted into Eq. (22), it can easily be deduced that $g_0\propto r^{1/2}$ in the limit $r\ll 1$. This scaling behavior is reproduced by the numerical calculations in Fig. 4. Figure 4 also shows that the numerical value of g_0 does not change very much as ψ_0 changes in the limit $r\ll 1$. To a very good approximation, we obtain the following empirical relation in the limit $r\ll 1$:

$$g_0 = -(0.44\pm 0.018)r^{1/2}. \tag{24}$$

(2) In the limit $r\gg 1$, we find that the magnitude of g_0 decreases proportional to r^{-1} for a symmetric bilayer. In this case, $\psi_n=0$ for all odd n, $\psi_1\sim 1$, and $\psi_3\propto r^{-1}$. g_0 in Eq. (22) does not contain a contribution due to ψ_1 and the first nonzero contribution is due to ψ_3, which is proportional to r^{-1}. In the case of an asymmetric bilayer, there is a nonzero contribution due to ψ_2, which is proportional to $r^{-1/2}$ from Eqs. (7)–(9). Due to this, g_0 tends to a constant value in the limit $r\gg 1$. This value is, however, numerically small for both the asymmetric bilayers with $\psi_0=0.25$ and 0.5 considered here.

In the limit $r\gg 1$, Eqs. (13)–(15) indicate that $\psi_n\sim r^{(-(n-1)/2)}$. From Eq. (21), the bending and compression moduli are both proportional to Ar in this limit,

$$B\sim (Ar),$$
$$K\sim (Ar/k^2). \tag{25}$$

In the limit $r\ll 1$, Eq. (18) indicates that $\psi_n\propto n^{-1}$. However, this scaling is cut off due to the gradient terms in expression (4) for the concentration field. For $g\sim r^{1/2}$, it was shown in the previous paragraph that the upper limit for n_c, which scales as $n_c\sim r^{-1/4}$ and the bending and compression moduli can be calculated using this upper cutoff for n, are

$$B = A\sum_{n} 4rn^4\psi_n^2 \sim Arn_c^3 \sim Ar^{1/4}, \tag{26}$$

$$K = A\sum_{n} (r/k^2)n^2\psi_n^2 \sim A(r/k^2)n_c, \tag{27}$$

$$\sim A(r^{3/4}/k^2). \tag{28}$$

The bending and compression moduli, scaled by (Ar), are shown as a function of the r in Figs. 5 and 6 for the zero surface tension case $g=g_0$, as well as for the case $g=0$. It is

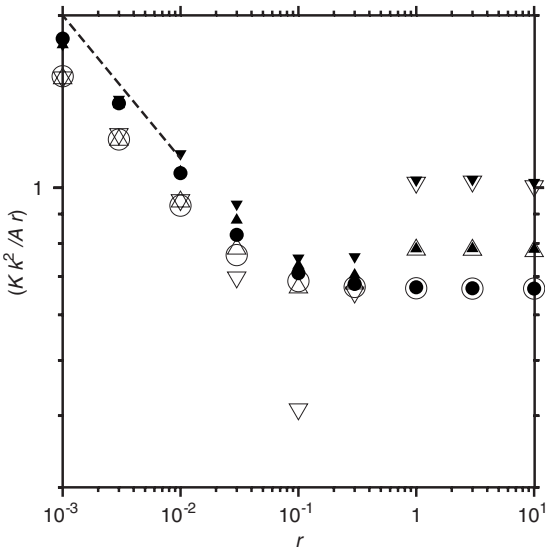

FIG. 6. The scaled bending modulus $(Kk^2/(Ar))$ for a symmetric bilayer (○), for an asymmetric bilayer with $\psi_0=(0.25/r^{1/2})$, for $r\geq 1$ and $\psi_0=0.25$, for $r\leq 1$ (△), and an asymmetric bilayer with $\psi_0=(0.5/r^{1/2})$ for $r\geq 1$ and 0.5 for $r\leq 1$ (▽). The filled symbols show the results for zero surface tension and the filled symbols show the results for $g=0$. The dashed line on the left shows the slopes of −0.25.

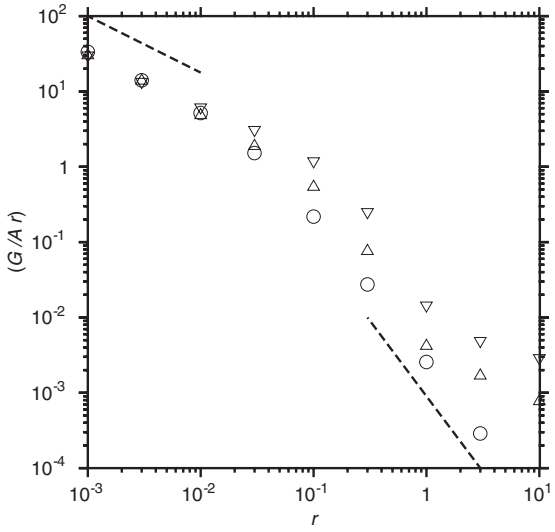

FIG. 7. The scaled surface tension $(G/(Ar))$ for a symmetric bilayer (○), for an asymmetric bilayer with $\psi_0=(0.25/r^{1/2})$ for $r\geq 1$ and $\psi_0=0.25$ for $r\leq 1$ (△), and an asymmetric bilayer with $\psi_0=(0.5/r^{1/2})$ for $r\geq 1$ and 0.5 for $r\leq 1$ (▽). The dashed line on the left shows a slopes of −0.75, while the dashed line on the right shows a slope of −2.

observed that both the (B/Ar) and $(Kk^2/(Ar))$ approach constant values in the limit $r\gg 1$, as anticipated in Eq. (25). In the limit $r\ll 1$, we found that (B/Ar) and (G/Ar) increase proportional to $r^{-3/4}$, while (Kk^2/Ar) increases proportional to $r^{-1/4}$, as obtained in Eqs. (26) and (27). For completeness, we also show the scaling behavior of the moduli for the case where $g=0$. There are several salient features of the variation in the scaled compression and bending modulus with the parameter r.

(1) In the limit $r\gg 1$, there is very little difference in the compression and bending moduli with the parameter g. Therefore, the compression and bending moduli are nearly equal for zero surface tension and for $g=g_0$. However, there is a significant variation in the bending and compression moduli with the parameter ψ_0.

(2) In the limit $r\ll 1$, there is very little variation in the bending and compression moduli with ψ_0, indicating that the scaled compression and bending moduli are largely independent of ψ_0. However, the scaled bending and compression moduli do depend on g and the moduli for the zero surface tension case are lower than those for $g=0$. Using the data available for $r<0.01$, we can obtain empirical correlations for the compression and bending moduli in the limit $r\ll 1$. For the zero surface tension case, the scaled bending and compression moduli are well represented by the following empirical relation in the limit $r\ll 1$:

$$(B/Ar) = (0.296 \pm 0.006)r^{-3/4}, \tag{29}$$

$$(Kk^2/Ar) = (0.282 \pm 0.002)r^{-1/4}. \tag{30}$$

For the case $g=0$, the bending and compression moduli are well represented by the following empirical relations in the limit $r\ll 1$,

$$(B/Ar) = (0.594 \pm 0.012)r^{-3/4}, \tag{31}$$

$$(Kk^2/Ar) = (0.326 \pm 0.005)r^{-1/4}. \tag{32}$$

Finally, we examine the nonzero value of the surface tension that would be obtained if parameter g was set equal to zero in the free energy functional (1). As already explained above, a lamellar phase has a zero surface tension because there is no energy penalty for tilting the bilayers. However, when the free energy functional (1) is used with $g=0$, there is a finite surface tension given in Eq. (21). It is of interest to examine whether this nonzero value is large or small, to determine whether the error due to the assumption $g=0$ is significant. The value of the scaled surface tension for $g=0$ is shown as a function of r in Fig. 7. It is observed that the surface tension decreases proportional to r^{-2} for a symmetric bilayer for $r\gg 1$, as reported earlier.[9] However, for an asymmetric bilayer, the surface tension saturates to a small nonzero value for $r\gg 1$. This value is numerically small for $\psi_0=(0.25/r^{1/2})$ and $\psi_0=(0.5/r^{1/2})$, but it is greater than zero, indicating that an asymmetric bilayer with $g=0$ has a small but nonzero surface tension. In the limit $r\ll 1$, we find that the scaled surface tension (G/Ar) increases proportional to $r^{-3/4}$, as in the case of the symmetric bilayer. The surface tension shows very little variation in value for $\psi_0=0.25$ and 0.5 and is well fitted by the approximate relation,

$$(G/Ar) = (0.179 \pm 0.007)r^{-3/4}. \tag{33}$$

C. Dynamics

The model-H equations for binary fluids have been used to model the mesoscale dynamics of symmetric lamellar phases.[9] Here, a relationship was obtained between the Onsager coefficient Γ in the mesoscale description and the permeation constant P in the equation for the relative motion between the fluid and the layers in the macroscopic descrip-

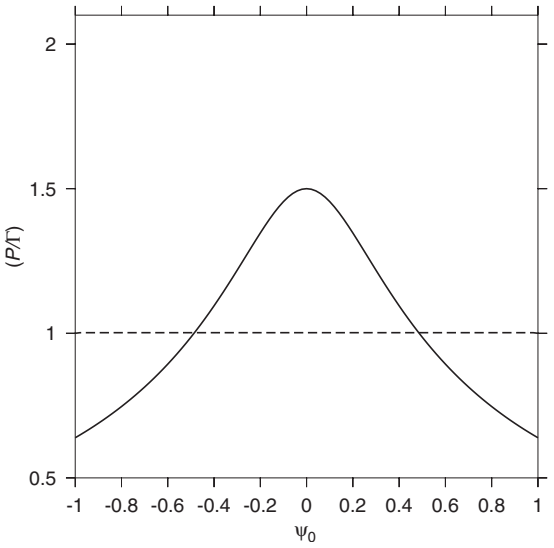

FIG. 8. The limiting values in of (P/Γ) as a function of $(\psi_0/r^{1/2})$ for $r \gg 1$ (solid line) and as a function of ψ_0 for $r \ll 1$ (broken line).

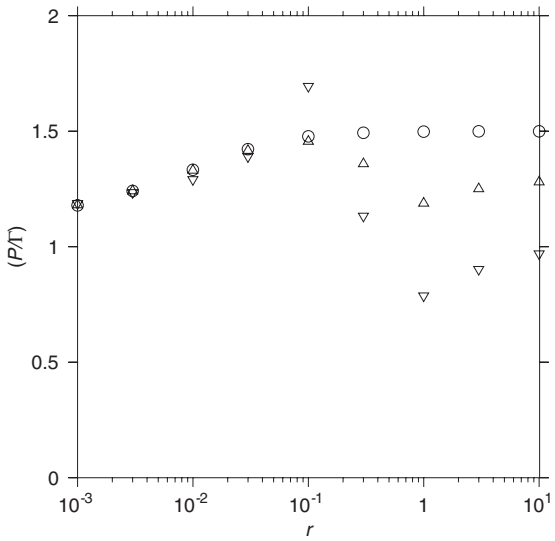

FIG. 9. The ratio (P/Γ) as a function of r for the case $g=0$ for a symmetric bilayer (○) and an asymmetric bilayer with $\phi_0=0.25$ (△) and an asymmetric bilayer with $\psi_0=0.5$ (▽).

tion. We do not provide the details here, but simply provide the final expression for the permeability in terms of the Onsager coefficient,

$$P = \frac{\Gamma}{\left(\Sigma_{n=-\infty}^{\infty} \psi_n^2\right)}. \tag{34}$$

In the earlier study of symmetric bilayers,[9] it was shown that the permeation constant in equation P has the same dimensions as the Onsager coefficient in equation Γ. The ratio (P/Γ) can be evaluated in the asymptotic limit $r \gg 1$ and $r \ll 1$ as follows. In the limit $r \gg 1$, the dominant contribution to the denominator of Eq. (34) is due to the coefficient ψ_1, since all higher coefficients are small. Therefore, (P/Γ) can be obtained using Eq. (11) for ψ_1 and neglecting all other coefficients. In the limit $r \ll 1$, the coefficients (18) can be used for the coefficients ψ_n, in order to obtain the ratio (P/Γ). These limiting values (Fig. 8) are shown as a function of the asymmetry ψ_0 in Fig. 2. In the limit $r \ll 1$, the numerical evaluation of Eq. (34), using Eq. (18) for the coefficients ψ_n, shows that (P/Γ) is exactly equal to 1 independent of ψ_0. For a symmetric lamellar phase, the ratio of the permeation constant and the Onsager coefficient tends to a constant value of 1.5 in the limit $r \gg 1$, where the amplitudes ψ_n are given by Eqs. (13)–(15).

The ratio (P/Γ) for an asymmetric lamellar phase is shown as a function of the parameter r for two different values of $\psi_0=0.25$ and $\psi_0=0.5$ in Fig. 9. This ratio varies in a very narrow range between about 0.7 and 1.5 for all the r values analyzed here. It is important to note that the ratio (P/Γ) remains finite in both limits $r \ll 1$ and $r \gg 1$ and shows a maximum in the intermediate regime for an asymmetric bilayer. This is in contrast with a monotonic increase for a symmetric bilayer. In the limit $r \ll 1$, it is observed that the value of (P/Γ) is independent of ψ_0, as expected from Fig. 2. However, the numerical value does not approach the asymptotic value $(P/\Gamma)=1.0$ even at $r=0.001$ and it is necessary to go to even lower values of r to get close to the asymptotic limit.

III. CONCLUSIONS

The relationship between parameters that can be obtained from a molecular simulation, such as the concentration, profile, bending, and compression moduli, and the parameters in a mesoscale free energy functional have been obtained for an asymmetric lamellar phase, in which the thickness of the water and surfactant layers are not equal. This follows an earlier study,[9] where similar parameters were obtained for a symmetric lamellar phase. The effect of asymmetry in the concentration field was incorporated using a cubic term in the free energy functional. The free energy functional minimized, and the resulting nonlinear equation for the concentration field were then expanded in a Fourier series [Eq. (5)], resulting in a set of simultaneous equations for the different Fourier modes. These were solved simultaneously to obtain the Fourier coefficients ψ_n, as well as the parameter c in the free energy functional. Due to the presence of a cubic term in the free energy functional, we find that all the Fourier coefficients are nonzero for an asymmetric bilayer. This is in contrast with the case of a symmetric bilayer, where all even Fourier coefficients, $\psi_0, \psi_2, \cdots$ are zero.

The sharpness of the interface, determined by the parameter r in the free energy functional Eq. (1), plays an important role in determining the dynamics of the system. In the limit $r \gg 1$, the concentration profile is close to a sine function. In this case, we see that the maximum asymmetry (difference in the mass fraction of the hydrophobic and hydrophilic parts) decreases proportional to $r^{-1/2}$. This is because the concentration profile reduces to a perfect sine wave in the limit $r \to \infty$ and a sine wave is symmetric. This indicates that the asymmetry in the concentration field, which can be modeled using the free energy functional Eq. (1), is limited in the limit $r \gg 1$, where the interface is very diffuse. There is no such limitation for the case $r \ll 1$, where the concentration profile tends to a series of step functions.

An issue of importance is the requirement, for a lamellar

phase, that the surface tension has to be zero. In the free energy functional, the zero tension state is achieved by incorporating a surface tension term proportional to g in the free energy functional. The surface tension is positive for $g=0$ and zero tension is achieved by setting $g=g_0$, where g_0 is negative. For a symmetric bilayer, it was found that g_0 decreased proportional to r^{-2} for a diffuse interface in the limit $r \gg 1$. For an asymmetric interface, we find that g_0 tends to a finite, but numerically small, value in the limit $r \gg 1$. The magnitude of g_0 increases as the asymmetry increases. In the limit $r \ll 1$ where there is a sharp interface, it is found that $|g_0| \sim r^{-3/4}$, and the numerical value of g_0 is remarkably insensitive to the asymmetry in the concentration profile.

The bending and compression moduli were determined in terms of the parameter r, which determines the sharpness of the interface, and the parameter A, which provides a measure of the energy per unit volume. In the limit $r \gg 1$, the scaled bending and compression moduli for an asymmetric bilayer are larger than those for a symmetric bilayer. However, in the limit $r \ll 1$ where the interface becomes sharp, there is very little dependence of the asymmetry on the bending and compression moduli. The permeation constant of the fluid through the bilayer was also determined in terms of the Onsager coefficient in the concentration equation in the mesoscale description. As in the case of symmetric bilayers, the ratio of the permeation constant and the Onsager coefficient tends to constant values both for $r \gg 1$ and $r \ll 1$ and varies in a small range between 0.7 and 1.5 in the intermediate regime.

The present analysis shows that the thermodynamic and dynamical properties of an asymmetric bilayer are sensitive to the asymmetry in the concentration for diffuse interfaces, where the concentration profile can be described by a sine wave. However, for sharp interfaces, the dependence of the thermodynamic and dynamical properties on the parameters in the free energy functional is not sensitive to the asymmetry in the concentration profile.

ACKNOWLEDGMENTS

The author would like to thank Professor K. G. Ayappa, Professor P. Maiti, and Professor Sriram Ramaswamy for interesting discussions. Financial support from Proctor & Gamble, USA is gratefully acknowledged.

[1] R. G. Larson, Rheol. Acta **32**, 245 (1993).
[2] H. A. Barnes, J. F. Sutton, and K. Walters, *An Introduction to Rheology* (Elsevier, New York, 1993).
[3] S. Chen and G. D. Doolen, Annu. Rev. Fluid Mech. **30**, 329 (1998).
[4] A. Xu, G. Gonnella, and A. Lamura, Phys. Rev. E **74**, 011505 (2006).
[5] F. Corberi, G. Gonnella, and A. Lamura, Phys. Rev. E **66**, 016114 (2002).
[6] G. Gonnella, E. Orlandini, and J. M. Yeomans, Phys. Rev. E **58**, 480 (1998).
[7] E. Orlandini, M. R. Swift, and J. Yeomans, Chem. Eng. Sci. **32**, 463 (1995).
[8] V. Kumaran, S. K. Jariwala, and S. Hussain, Chem. Eng. Sci. **56**, 5663 (2001).
[9] V. Kumaran, Y. K. V. V. N. Krishna Babu, and J. Sivaramakrishna, J. Chem. Phys. **130**, 114907 (2009).
[10] O. Stenull, Phys. Rev. E **78**, 031704 (2008).
[11] G. Basappa, Suneel, V. Kumaran, P. R. Nott, S. Ramaswamy, V. M. Naik, and D. Rout, Eur. Phys. J. B **12**, 269 (1999).
[12] M. Zapotocky, L. Ramos, P. Poulin, D. A. Weitz, and T. C. Lubensky, Science **283**, 209 (1999).
[13] M. Kleman, *Points, Lines and Walls in Anisotropic Fluids and Ordered Media* (Wiley, Chichester, 1983).
[14] P. C. Hohenberg and B. I. Halperin, Rev. Mod. Phys. **49**, 435 (1977).